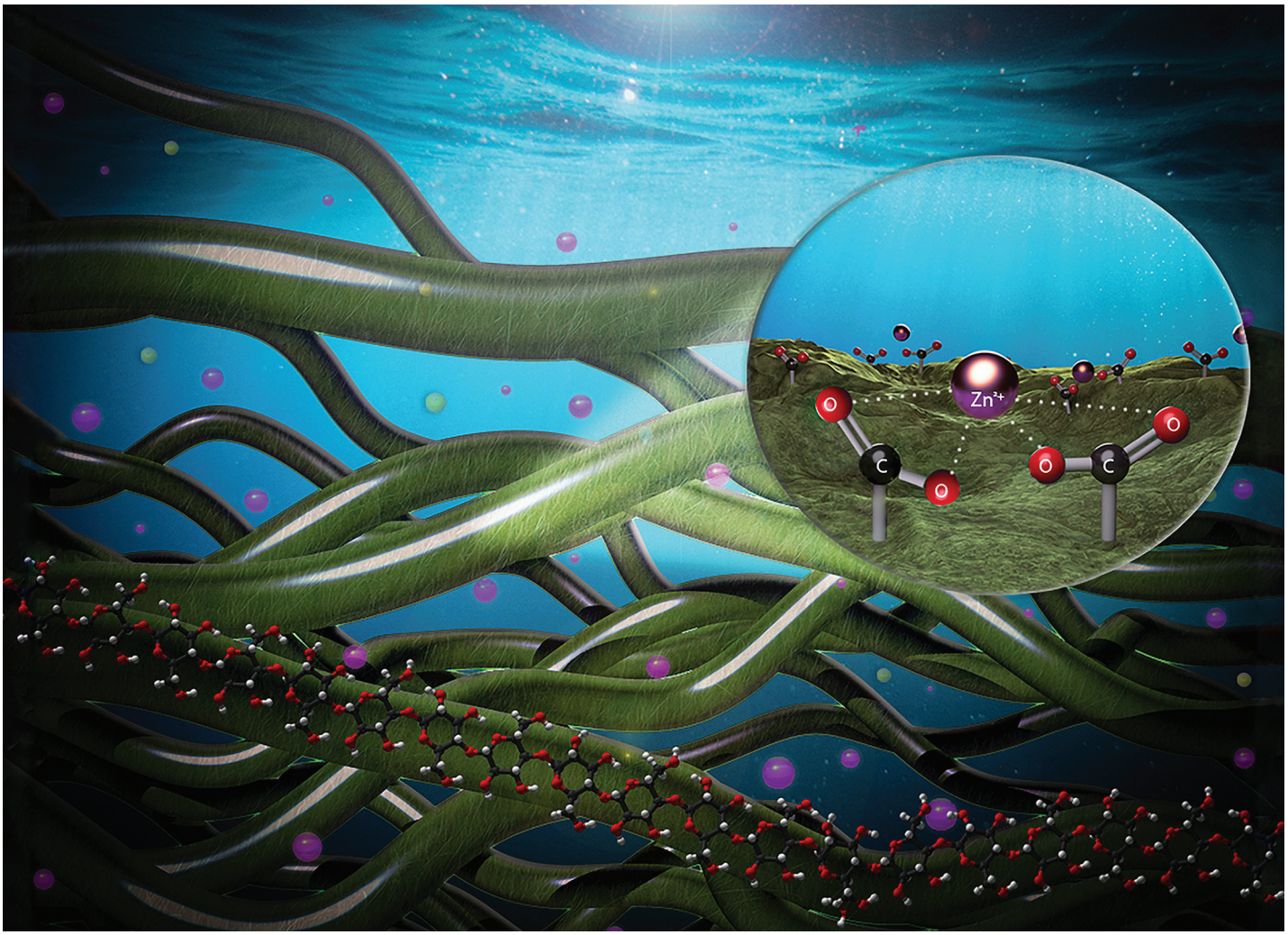

Showcasing research from Prof. Krassimir P. Velikov and Prof. Aji P. Mathew's groups at Unilever Innovation Centre Wageningen, Wageningen, the Netherlands and Division of Materials and Environmental Chemistry, Stockholm University, Stockholm, Sweden, respectively.

Multivalent ion-induced re-entrant transition of carboxylated cellulose nanofibrils and its influence on nanomaterials' properties

The carboxylated cellulose nanofibrils hydrogel is shown to undergo a re-entrant behaviour, where the gel strength abruptly increases and then decreases back, upon monotonic increase in multivalent counter-ions concentration. The behaviour is translated in the physical properties of 2D-films, prepared from hydrogels, providing new strategies to design novel functional biomaterials, with tuneable properties, by simply controlling the multivalent ion concentration in the hydrogels.

As featured in:

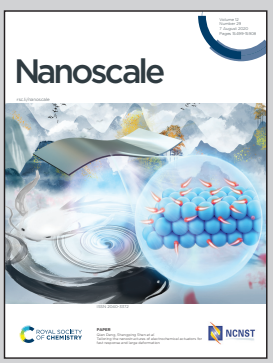

See Sugam Kumar, Krassimir P. Velikov *et al.*, *Nanoscale*, 2020, **12**, 15652.

ROYAL SOCIETY OF CHEMISTRY

rsc.li/nanoscale

Registered charity number: 207890

Nanoscale

ROYAL SOCIETY OF CHEMISTRY

PAPER

View Article Online
View Journal | View Issue

Cite this: *Nanoscale*, 2020, **12**, 15652

Multivalent ion-induced re-entrant transition of carboxylated cellulose nanofibrils and its influence on nanomaterials' properties†

Luis Valencia, ‡[a,b] Emma M. Nomena, ‡[c,d] Susanna Monti, ‡[e] Walter Rosas-Arbelaez,[f] Aji P. Mathew, [a] Sugam Kumar *‡[a,g] and Krassimir P. Velikov *[c,d,h]

In this work, we identify and characterize a new intriguing capability of carboxylated cellulose nanofibrils that could be exploited to design smart nanomaterials with tuned response properties for specific applications. Cellulose nanofibrils undergo a multivalent counter-ion induced re-entrant behavior at a specific multivalent metal salt concentration. This effect is manifested as an abrupt increase in the strength of the hydrogel that returns upon a further increment of salt concentration. We systematically study this phenomenon using dynamic light scattering, small-angle X-ray scattering, and molecular dynamics simulations based on a reactive force field. We find that the transitions in the nanofibril microstructure are mainly because of the perturbing actions of multivalent metal ions that induce conformational changes of the nanocellulosic chains and thus new packing arrangements. These new aggregation states also cause changes in the thermal and mechanical properties as well as wettability of the resulting films, upon water evaporation. Our results provide guidelines for the fabrication of cellulose-based films with variable properties by the simple addition of multivalent ions.

Received 11th April 2020,
Accepted 26th May 2020

DOI: 10.1039/d0nr02888f

rsc.li/nanoscale

Introduction

In recent years, nanocellulose (NC) has been used as building-block in the development of multifunctional materials not only because of its abundance and biodegradability but also because of its outstanding inherent properties, such as high mechanical strength, tuneable self-assembly and reinforcing capabilities.[1–6] Moreover, NC properties can be modified and modulated depending on the required material performance *via* different forms of pre-treatments or surface-modification techniques.[7,8] For example, TEMPO (2,6,6-tetramethylpiperidine-1-oxyl radical) mediated oxidation of cellulose nanofibrils (CNF) results in the formation of the TEMPO-oxidized CNF (TOCNF) having a high content of carboxyl groups. TOCNF is a hydrogel even at low solid content, which upon drying forms durable and highly-transparent materials.[9] TOCNF has readily found application in a wide range of fields, such as in biomedicine,[10] flexible electronics,[11] and water/gas purification.[7,12–14] The high gel-strength of TOCNF is mainly arising from the high aspect ratio of the nanofibrils that generates inter-connected entanglements, besides complex interplay of various interactions such as hydrophobic, electrostatic, van der Waals interactions as well as hydrogen bonding.[15,16]

As in all polyelectrolyte hydrogels, the viscoelastic properties of TOCNF also depend on the swelling and collapse of the network, induced by the ions present in solution. The behaviour of polyelectrolyte gels in the presence of ions is mostly described by the Donnan model, or other theories like Debye–Hückel (DH), usually used to predict the stability of charged colloids in ion solutions. The Donnan effect assumes a concentration imbalance between the ions inside the gel and in the bulk solution, leading to a partial swelling as promoted

[a]*Division of Materials and Environmental Chemistry, Stockholm University, Frescativägen 8, 10691 Stockholm, Sweden. E-mail: sugamkumar86@gmail.com*
[b]*Materials Technology and Chemistry, Alfa Laval Tumba AB, SE-14782 Tumba, Sweden*
[c]*Unilever Innovation Centre Wageningen, Bronland 14, 6708 WH Wageningen, The Netherlands. E-mail: krassimir.velikov@unilever.com*
[d]*Institute of Physics, University of Amsterdam, Science Park 904, 1098 XH Amsterdam, The Netherlands*
[e]*CNR-ICCOM – Institute of Chemistry of Organometallic Compounds, via Moruzzi 1, 56124 Pisa, Italy*
[f]*Department of Chemistry and Chemical Engineering-Applied Chemistry, Chalmers University of Technology, SE-41296 Gothenburg, Sweden*
[g]*Solid State Physics Division, Bhabha Atomic Research Centre, Mumbai, 400 085, India*
[h]*Soft Condensed Matter, Debye Institute for Nanomaterials Science, Utrecht University, Princetonplein 5, 3584 CC Utrecht, The Netherlands*

†Electronic supplementary information (ESI) available. See DOI: 10.1039/d0nr02888f

‡Equal contribution from the authors.

to maximize the translational entropy of the ions. On the other hand, DH theory considers the formation of counter-ion clouds around the colloidal particles, suppressing the electrostatic repulsion between them and hence causing the gel to collapse. However, all these classical theories provide similar outcomes and are only able to account for monotonic phase transitions (*e.g.* volume transitions such as swelling-to-collapse or *vice versa*) in gels. They do not predict any of the so-called re-entrant transitions, where the system transforms from the initial phase to another one but then completely or partially returns to the initial phase with a monotonic increase in some physicochemical parameter (*e.g.* swelling-to-collapse-to-swelling).

Recently, there have been many studies reporting different re-entrant transitions in a variety of colloidal systems including DNA, proteins, and nanoparticles in the presence of multivalent ions.[17–19] Multivalent ions are known to give rise to several counterintuitive phenomena (*e.g.* over-changing of colloids, like charge-attraction, re-entrant stabilization)[20–22] which are in contradiction of the theoretical understanding, limiting in great extent the validity of classical theories. Such deviations from well-established theories are believed to be emerging from correlations between ions as well as between ions and colloidal particles. These correlations are predominantly observed in biological systems where the charge distribution is complex and non-uniform. Nevertheless, in the case of polyelectrolyte gels, a re-entrant volume transition (swelled-to-collapse-to-swelled state) in the presence of multivalent ions has been theoretically predicted by taking into consideration ion-ion correlations as accounted by short-range electrostatic, excluded volume and hard-sphere interactions.[18,23] There are a few studies investigating the multivalent ion-mediated gelation of TOCNF,[24–27] correlating the moduli of the hydrogels to both the electronic structure of metal cations and their binding strengths with carboxylate groups. However, to the best of our knowledge, none of them until now has shown any re-entrant transition in CNF.

In this work, we demonstrate a re-entrant transition of TOCNF hydrogel where the gel-strength abruptly increases and then decreases back upon an increase in metal salt concentration. The re-entrant behaviour is manifested in the variation of the storage modulus (G') with increasing salt concentration, where G' shows a maximum value at a particular salt concentration (hereafter denoted as critical salt concentration, C_0), whereas the value of G' decreases, for salt concentrations, more and less than C_0. Such a transition is observed with multivalent metal counter-ions only while the storage modulus shows a monotonic increase with a monovalent metal salt, in the measured concentration range. Zinc ions (Zn^{2+}) are used as a model system for most of the study, however, we corroborated our observations by examining other metal ions too, namely Al^{3+} and Ca^{2+}. The structural and dynamical transformations of TOCNF during the re-entrant transition were probed by small-angle X-ray scattering (SAXS) and dynamic light scattering (DLS). The results suggests the re-entrant transformation at the micro-structure and micro-dynamical level.

Moreover, molecular dynamics simulations (Reactive Force Field, or ReaxFF) were carried out to examine the environment of the counter-ions near the CNF. Combining all the data, we provide a coherent picture of the observed phenomenon and propose a plausible mechanism for the re-entrant transition of TOCNFs. Furthermore, the influence of the different aggregation states on the properties of dried films was elucidated, proving the existence of a re-entrant phenomenon in the thermal and nano-mechanical properties of the resulting films, as well as their wettability.

Experimental details

Materials

High-purity cellulose from softwood fibres (Norwegian spruce) with high cellulose content (95% cellulose, 4.5% hemicellulose, and 0.1% lignin content provided by Domsjö Fabriker AB, Sweden) was used as starting material to produce cellulose nanofibers. 2,6,6-tetramethylpiperidine-1-oxyl radical (TEMPO), sodium bromide (NaBr), sodium hypochlorite (NaClO), zinc chloride ($ZnCl_2$), aluminum chloride ($AlCl_3$), sodium chloride (NaCl) and calcium chloride ($CaCl_2$) were purchased from Sigma-Aldrich (Germany). Deionized water was used for the preparation of all solutions.

Fabrication of TOCNF

TOCNF was produced *via* defibrillation process of soft-wood pulp, following previously reported procedures by Isogai *et al.*[28,29] In brief, an aqueous pulp suspension from Norwegian spruce is subjected to TEMPO-mediated oxidation using TEMPO, NaClO and NaBr. The obtained carboxylated fibres were then subjected to mechanical disintegration using a high-pressure homogenizer operated at 500 bars (5 passes) to produce fully defibrillated TOCNF.

Preparation of TOCNF films

TOCNF films were prepared by solvent-evaporation, where 40 g of TOCNF aqueous suspensions (0.2 wt%) at different salt concentrations, were poured into plastic Petri dishes after degassing to remove any presence of bubbles and dried in an oven at 35 °C for 24 h.

Characterization

Properties of TOCNF. The TOCNF exhibited a diameter of 5–20 nm and a length of 1–2 μm (determined by Atomic Force Microscopy, see details below). The surface charge (negative) density of TOCNF was determined by conductometric titration and found to be 1.2 mmol g_{TOCNF}^{-1}. For the titration, first, 0.2 g of TOCNF was suspended in 20 mL of water. The pH of the solution was adjusted to 2.5 by adding HCl (0.1 M). Then, the suspension was titrated with 0.1 M NaOH. To estimate the carboxyl groups per glucose, ^{13}C solid-state NMR experiments of TOCNF were performed with a Bruker AVANCEIII spectrometer and a magnetic field of 14.1 T, with a probe size of 4 mm. The chemical shifts are quoted relative to neat tetra-

methylsilane (TMS). Settings: spinning speed 14 kHz, number of scans 13 000, relaxation delay 2.5 s, cross-polarization contact time 1.1 ms. A variable amplitude cross polarization ramp range of 20% to a maximum amplitude of 43 kHz during contact time was used. During the acquisition period, the protons were decoupled using a SPINAL-64 ^{1}H decoupling.

Rheology measurements. Rheology was performed on a MRC301 rheometer (Anton Paar, Germany) at 20 °C using either a sandblasted 40 mm parallel plate geometry with a 1 mm gap or a 27 mm Couette geometry depending on the sample. Samples were carefully loaded using a plastic spoon in accordance with instrument guidelines. Amplitude strain sweeps and frequency sweeps were performed to determine the range of the linear viscoelastic region. A time sweep was performed for 5 minutes, measuring G' and G'' at 0.1% strain and a frequency of 1 Hz.

Zeta (ζ) potential measurements. The electrophoretic mobility and ζ-potential of the TOCNF samples were measured using Zetasizer Nano ZS (Malvern Instruments, UK) instrument, employing a dip-cell kit and plastic cuvettes. Samples (0.2 wt% TOCNF suspensions with salts) were diluted in 1 : 50 prior to these measurements, where the salts concentrations are normalized with respect to C_0 by rheology. It may be clarified that dilution does not alter the trends in the measured properties or system characteristics, as also verified by rheology.

Microscopy. The morphology and roughness of the TOCNF dried films were determined with a MultiMode 8 Atomic Force Microscope (AFM, Bruker, NanoScope controller, USA). The height, amplitude and phase images were recorded using a ScanAsyst-Air probe in peak force tapping mode. The collected data were processed with the software NanoScope Analysis 1.5 (Bruker). Confocal laser scanning microscopy (CLSM) was performed to visualize the microstructure of the gels. The gels were stained with Direct yellow (Solophenyl Flavine 96 at 0.5 wt%) by adding a drop of the dyes to about 1 g of gel. A drop of the resulting mix was then placed on a cover slip and micrographs of the emulsions were acquired using a Leica TCS-SP5 and DMI6000 inverted microscope (Leica GmbH, Germany). Fluorescence from the samples was excited at 488 nm for Direct Yellow, emission was detected at 496–555 nm. A 63× oil-immersion objective was used to scan the images at approximately 30 μm below the cover slip.

Small angle X-ray scattering. The TOCNF hydrogels (0.2 wt% with salts) were diluted in 1 : 2 prior to the measurements and incorporated into glass capillaries. SAXS measurements were carried out using Mat:Nordic instrument from SAXSLAB. The setup used was equipped with a Rigaku high brilliance microfocus X-ray source with CuK_α radiation. The sample was placed in a capillary holder in an evacuated sample chamber and the entire space between collimator and detector was evacuated to minimize air scattering. A Pilatus 300 K detector was used to record the scattering intensity. The sample-to-detector distance was about 1085 mm, with a beam size of 0.3 mm. The measured SAXS data were analysed using model dependent data analysis procedure where the experimental data is compared with the model scattering. The fitted parameters were optimized using the nonlinear least-squares method.

Dynamic light scattering. DLS measurements were performed using Zetasizer Nano ZS (Malvern Instruments, UK) instrument. The samples (0.2 wt% TOCNF suspensions with salts) were diluted in 1 : 50 prior to the measurements. In DLS, one investigates the fluctuations in the intensity of scattered light by particles, dispersed in a medium. These fluctuations are detected and analysed to extract the information about the dynamics that can be correlated to the structure as well as interactions in the system. The fluctuations are quantified in terms of the normalized autocorrelation function (ACF) $[g^{(2)}(\tau)]$ of the scattered light intensity, which for monodisperse spherical scatterers can be expressed as[30]

$$g^{(2)}(\tau) = \beta e^{-2\Gamma\tau} + A \quad (1)$$

where τ denotes the delay time in the ACF, A is the baseline while β ($0 < \beta < 1$) is the spatial coherence factor decided by the optical geometry of the instrument/experiment. Γ represents the relaxation rate or decay constant, defining the time scale of the motion present in the system, in terms of the translational diffusion coefficient (D) of the particles.

Computational simulations. For the model building, an equilibrated model of CNF (Fig. S1 and 2†), consisting of sixteen chains made of sixteen glucosyl residues each, assembled as a parallelepiped rod (approximately 84 × 25 × 25 Å^3), which was used previously to investigate composite CNF-graphene oxide materials,[7] was modified to reproduce the experimental conditions of this study by replacing certain amount of the $-CH_2OH$ groups of the chains (following the ^{13}C SS NMR results, Fig. S3†) exposed to the solvent with carboxyl moieties (from the TOCNF).[29,31] The resulting negatively charged system was then neutralized by adding Na^+ counterions and solvated by surrounding it with approximately 15 000 water molecules (simulation box size: 84 × 101 × 54 Å^3). The dimensions of the simulation box were adapted to match the solvent density, during preliminary equilibrations in the NPT ensemble at T = 300 K. Periodic boundary conditions were applied in all directions in such a way that the replication along × emulated a continuous infinite nanofiber.

As already commented,[32] the chosen sizes (fibre and box) were appropriate to generate a reasonable variety of configurations at different $ZnCl_2$ concentration useful for explaining and predicting the experimental data at different concentrations. Based on the storage modulus plot (Fig. 2a, discussed later), three Zn^{2+}/COO^- ratios, representing the different salt concentrations (Table S1†), were selected and simulated extensively for tens of nanoseconds.

The initial structure of the fibre, in all the simulated cases, was obtained by extracting an average configuration of the whole system from the last portion of the production trajectory where the nanofibril arrangements were explored in water + neutralizing Na^+ counter-ions only. To create the new models, some of the water molecules relatively close to the nanofiber were randomly replaced with Zn^{2+} and Cl^- ions, preserving the

original number and location of the Na^+ ions (Fig. S4†). Six different initial starting configurations were generated, in each case, and simulated for times varying from 3 to 5 ns, which were sufficient to obtain relatively stable ion distributions. To increase sampling, a few configurations were extracted during the production dynamics and used as the starting geometries of other nanosecond simulations.

The last portions of the trajectories were then used for the final analysis. The systems were first equilibrated in the NPT ensemble at $T = 300$ K with constraints, freezing the solute and the x dimension of the box, and then without constraints removing just the solute restrictions. Subsequently, the MDs were extended, and production trajectories were carried out in the NVT ensemble saving the structure every 0.4 ps. The temperature was controlled through the Berendsen's thermostat[33] with a relaxation constant of 0.1 ps and the time step was set to 0.5 fs. All reactive molecular dynamics runs were based on a previous parametrized force field tuned for these systems.[32] All MD simulations were carried out with the ReaxFF code available in the Amsterdam Density Functional (ADF)/ReaxFF package[56] installed on local clusters and workstations (at CNR-IPCF/ICCOM) but also with the LAMMPs package available at the CINECA supercomputing centre (high-performance computing resources – ISCRA initiative). Additional details on the computational simulations can be found in ESI.†

Physical properties of films. The thermal behaviour of the TOCNF films was assessed by thermogravimetric analyses (TGA) using TA Instruments Discovery thermal analyser, measuring the mass transformation as a function of temperature, in an interval of 30–600 °C, at a heating rate of 5 °C min^{-1}. The samples were exposed to nitrogen gas at a flow rate of 20 ml min^{-1}. The uniaxial mechanical properties of the films were measured through a tensile test using an Instron mechanical testing machine at a crosshead speed of 1 mm min^{-1} with a gauge length of 20 mm. The measurements were carried at 50% humidity and 25 °C temperature. The reported results were the average of calculating five specimens per sample. The surface hydrophobicity of the films was determined by the sessile drop using a goniometer (Drop Shape Analysis System, DSA100, Kruss GmbH, Germany). A water droplet was deposited onto the films and monitored for 60 s using a digital camera. Then, the contact angle was the angle between the film surface and the tangent line at the contact point with the droplet. DMT modulus of the TOCNF films was measured by a FastScan AFM (Bruker, NanoScope V controller, Santa Barbara, California, USA) Standard ScanAsyst.

Results and discussion

The infiltration of different concentrations of zinc salt ($ZnCl_2$) in TOCNF (0.2 wt%) suspensions rapidly triggers gelation resulting in the formation of homogenously turbid hydrogels. The metal ions interact with the cellulosic hydrogels by a combination of electrostatic interactions and dative covalent coordination bonds (Fig. 1).[34] It should be clarified here that

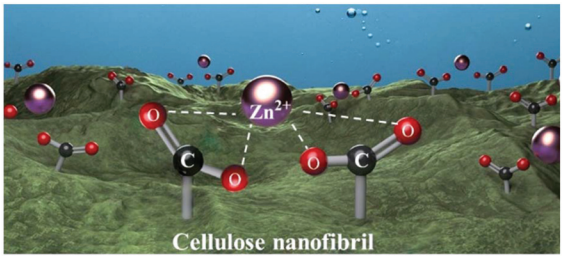

Fig. 1 Conceptual schematic illustration of the coordination complex formed between carboxylated cellulose nanofibrils and multivalent metal ions (Zn^{2+}).

for all the investigated samples, the storage modulus (G') is higher than loss modulus (G'') over the entire angular frequency range, suggesting characteristics typically associated with gels. Interestingly, while analysing the influence of the salt concentration on the rheological properties of TOCNF, we identify a non-monotonic behaviour in the storage modulus (G') upon a monotonic increase in the salt concentration (Fig. 2a), in the presence of multivalent ions only, denoting the generation of an ion-induced re-entrant transition. The process shows, first, a slow increase in G' as the salt concentration increases. Then, at a salt concentration of 2 mM (critical salt concentration, C_0), G' attains a maximum value, which is an order of magnitude higher than that of the reference material (TOCNF with no added salt). The increase in G' (displayed in Fig. 2a) is very sharp and abrupt. Upon further

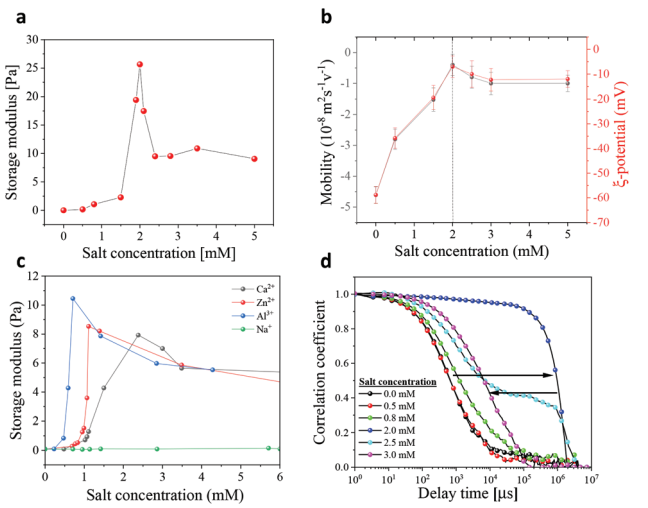

Fig. 2 Ion-induced re-entrant transition of TOCNF gel. (a) G' of a TOCNF suspension (0.2 wt%) as a function of salt (Zn^{2+} ions) concentration at 1 Hz and 0.1% strain. (b) Electrophoretic mobility and ζ-potential of TOCNF as a function of salt (Zn^{2+} ions) concentration. (c) G' of TOCNF suspensions (0.1 wt%) as a function of concentration of different metal salts at 1 Hz and 0.1% strain. (d) Auto-correlation functions of TOCNF (0.2 wt%) suspension as measured by DLS at different salt ($ZnCl_2$) concentrations. The arrows towards right and left show the decrease and increase in the decay time with an increasing salt concentration across the critical concentration (C_0).

increase in the salt concentration, G' decreases sharply until reaching a plateau that is however higher than the initial value of G' without salt. It should be noted that the re-entrant transition is very sharp and occurs across a quite small window of salt concentration. It is also important to mention that any variation in the surface charge density and/or sizes of the nanofibrils could slightly alter the exact C_0 value, and therefore should always be investigated per batch.

Further addition of salt does not significantly impact the storage modulus, which remains almost constant. A similar pattern can also be observed in the electrophoretic mobility as a function of the salt concentration displayed in Fig. 2b. As it is observed in Fig. 2b, the electrophoretic mobility of the reference system [no added $ZnCl_2$ salt (0 mM)] is approximately -4.8×10^{-8} m^2 s^{-1} v^{-1} and increases gradually with salt addition until it reaches approximately -0.4×10^{-8} m^2 s^{-1} v^{-1} at 2 mM. Further addition of salt induces a slight decrease in the electrophoretic mobility that tends to a plateau at approximately -1×10^{-8} m^2 s^{-1} v^{-1}. It may be noted that for the 0.2 wt% CNF dispersion, both maximum G' and maximum in the zeta potential (*i.e.* minimum negative value) was observed at 2 mM Zn^{2+}, suggesting that the C_0 correlates with the critical zeta potential of the system.[35] Noteworthy, although the pH of the TOCNF suspensions vary after the first addition of metal salt solutions, no significant variation in the pH is recorded at higher salt concentrations (Fig. S5†).

Additionally, to confirm the reliability of these observations, the response of TOCNF to other multivalent cations, namely Ca^{2+} and Al^{3+}, was also explored. The re-entrant behaviour was also observed in these cases, demonstrating the universality of the phenomenon. These measurements were performed also with 0.1 wt% TOCNF, where the highest storage modulus is obtained approximately at 1 mM for $ZnCl_2$. Both storage and loss modulus at these conditions are reported in Fig. S6.† However, the critical salt concentration, as well as the maximum value of the modulus (observed at critical salt concentration), decreases following the order (Al^{3+} > Zn^{2+} > Ca^{2+}). The variation in the G' as a function of equivalent ionic strength (up to 12 mM), corresponding to the respective salt concentrations is depicted in Fig. S7.† The observations confirm the validity of the approach and suggest a correlation of the binding strength between inter-fibril connections promoted by the bridging metal ions, with the ions' nature.[24] Nevertheless, for monovalent metal ions (Na^+ in Fig. 2c), the G' increases monotonically in the measured concentration range, in agreement with the classical theories, suggesting that the re-entrant transition only emerges with multivalent metal counter-ions. It is however important to note here that in the case of NaCl, aggregation of TOCNF may initiate at much higher NaCl concentration (≥50 mM), beyond the our measured NaCl concentration range, as reported by other studies, investigating rheological properties of TOCNF with varying NaCl concentration up to very high concentrations.[26,36] However, these studies have not shown any sort of re-entrant behavior in any of the measured properties with monovalent salt. Moreover, the re-entrant behavior in several other similar systems (*e.g.* DNA, proteins, viruses *etc.*) could only be observed with multivalent ions.[37–42] It is understood that the re-entrant behavior mostly arises because of ion-ion and/or ion-macroion correlations, which have much stronger influences, in the case of multivalent ions.[22,39,43,44]

The variation in the storage modulus can be corroborated to a transition of the hydrogels from a more liquid-like state to a solid-like state and return to liquid-like state (noticeably, less liquid-like compare to initial state as the G' in the re-entrant regime is more than that in initial low salt concentration regime) as the storage modulus provides a measure of elastic response of a material. Moreover, the storage modulus is also associated with the cross-linking degree, which in turn inversely related to the swelling of the gel, suggesting a swelling-to-deswelling-to-swelling transition.[18,23]

The dynamics of the system during the re-entrant transition was characterized using DLS which measures the collective diffusion related to the time dependence of the concentration fluctuations. The ACF of the TOCNF samples at different salt ($ZnCl_2$) concentrations are presented in Fig. 2d. A clear shift in the diffusive relaxation to a longer relaxation time (indicated by the right arrow) is observed upon addition of salt up to the critical salt concentration (C_0), endorsing the transition of the system from more dispersed (liquid-like) state to a condensed (solid-like) state.[19,30] This is essentially a first stage where the decay time of the correlation functions progressively increases as a function of salt concentration and reaches a maximum at C_0 (2 mM) with the highest storage modulus (Fig. 2a). Further increase in salt concentration (>C_0) causes a progressive decrease in the decay time of the correlation functions towards the original values (arrow pointing to the left), suggesting a transformation from condensed (more solid-like) state to a relatively more dispersed state. Interestingly, at a salt concentration around 2.5 mM, a bimodal distribution is obtained for ACF, which can be probably ascribed to an intermediate state of the phase transition, probably governed by two processes, the relaxation of the concentration fluctuations determined by the fast movement of the particles (the fast decay), and the decorrelation of the network topology (the slow decay).[17]

SAXS was used to disclose the structural evolution of TOCNF driven by the ions during the re-entrant transformation. The samples (0.2 wt% TOCNF suspensions with salt) were diluted by a factor of two, prior the measurements. Fig. 3 displays the SAXS data of the TOCNF hydrogels with varying salt concentrations. In SAXS, one measures the intensity of the scattered X-rays by the sample in the beam as a function of the magnitude of the scattering vector [($Q = 4\pi \sin(\theta)/\lambda$), where λ is the wavelength of the incident X-ray, and 2θ is the scattering angle], and the resulting scattering profiles are related to the structure and interactions of the system.[45]

All the plots show typical power-law behaviour of the scattering from the gels and/or correlated systems, in general.[46,47] The scattering profile of the sample without any additional salt (concentration ~0 mM) shows a slope of around Q^{-4}, in the low Q region, indicating the existence of a densely and uniformly packed homogeneous system. Upon addition of Zn^{2+}

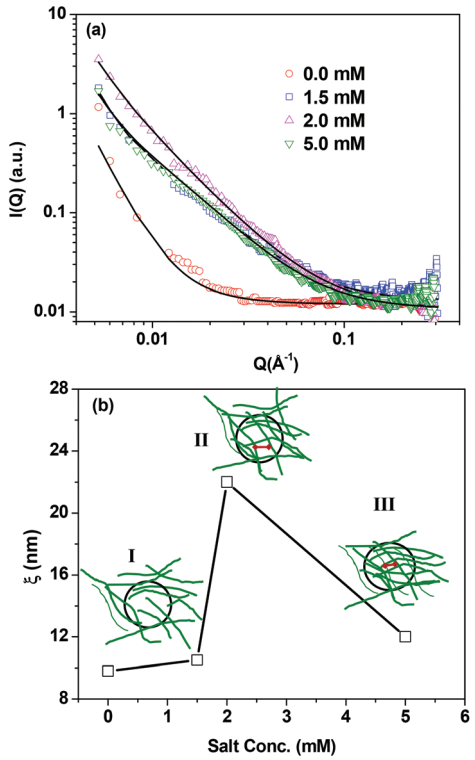

Fig. 3 (a) SAXS data of TOCNF hydrogels with varying salt concentrations, (b) variation in the correlation length (ξ) as a function of salt concentration.

ions, a scattering build-up with an approximate Q^{-2} dependence can be observed mainly in the intermediate Q range, indicating the formation of a more fractal-like structure.[38] The scattering profile changes its features while increasing salt concentration from 1.5 mM to critical salt concentration (*i.e.* 2 mM). Interestingly, on further increase in the salt concentration, to 5 mM (after C_0), the scattering profile matches with that observed at 1.5 mM (before C_0), consistent with the re-entrant transition of the hydrogels.

The SAXS data is analysed employing traditional two stage network model of the polymer gels,[46,47] comprising two terms as described in the following equation below:

$$(Q) = \frac{I_{OZ}(0)}{(1 + Q^2 \times \xi^2)} + \frac{I_{DB}(0)}{(1 + Q^2 \times \Xi^2)^2} \quad (2)$$

$I(0)$ denotes the forward scattering corresponding to the two terms.

The first term is a Lorentzian function, called as Ornstein–Zernike equation which describes the scattering caused by the compositional fluctuations, and the Fourier transform of it gives correlations, mathematically described by following exponentially dying out formula:[46,47]

$$\gamma(r) = \frac{1}{r}\exp(-r/\xi) \quad (3)$$

where, ξ is known as correlation length of the system and r is the distance between monomers. The space characterized by ξ is often described as a blob where the excluded volume effects are observed.[46,47]

On the other hand, the second term is the square of the Lorentzian function, known as Debye–Bueche function and usually used to describe the larger solid like inhomogeneities in the sample, where Ξ is the characteristic size of these inhomogeneities.[46] Since, no low Q cut off is observed in the SAXS data, implying that the size of these inhomogeneities is larger than that can be seen in the limited Q range of the measurement, therefore, we replaced second term by a simple power law accounting for the large moieties present in the sample.

$$I(Q) = \frac{I_{OZ}(0)}{(1 + Q^2 \times \xi^2)} + \frac{I_1}{Q^{-n}} \quad (4)$$

I_1 is a Q independent term, proportional to specific surface area, and n is the Porod exponent.[45]

The fitted correlation lengths of the system at different salt concentrations are shown in the inset of Fig. 3b where the inset schematics demonstrate the typical variation of the correlation length. The trend is remarkably similar to that observed in the storage modulus, suggesting that the changes in correlation length can be corroborated to the changes in rheology. It is worth mentioning here that both parameters (correlation length and storage modulus) are related to the cross-linking/networking formed by the fibrils in the system.

Without any additional salt, the system is highly homogenous and consists of uniformly distributed fibrils. The system in this case is believed to be containing individual fibrils with less entanglements, as the observed G' is very low for 0 mM of $ZnCl_2$, and as also suggested by Zhou *et al.*[48] The addition of salt ($ZnCl_2$) gives rise to network/entanglement formation among the nanofibrils, mostly *via* cross-linking through the metal cations.[24] As the salt concentration is increased to values lower than C_0, the fibrils get closer, and a slight increase in the correlation length is observed. At the critical salt concentration (C_0), the fibrils now form a network structure which is uniformly distributed throughout the gel and hence the maximum correlation length. Such strongly networked structure determines an increase in the storage modulus (solid-like character) of the system. Further increase in the salt concentration ($>C_0$) may lead to two possibilities (i) aggregation continues to enhance or (ii) suppression of the fibrils' aggregation. In the first case, the enhanced aggregation may lead to the formation of small coagulated clusters of the fibrils, where the fibrils are close to each other, giving rise to decreased correlation length. One of such clusters is shown in the stage III in Fig. 3(b). However, these clusters are sufficiently apart from each other, due to reduced number density, causing a significant decrease in G'. In the second possibility, the aggregation is believed to be suppressed on further increase in the salt concentration, probably because of rebalancing the interactions present in the system. Indeed, in the case of the polyelectrolyte gels, a similar phenomenon (swelling-to-deswelling-to-swelling) has been predicted and ascribed to the correlations among the ions, dominating at

higher salt concentrations[23] and particularly with multivalent ions. In several other systems also, such suppression of aggregation at higher multivalent salt concentration has been reported, due to the ion-ion correlations.[37–42]

A possible characterization at the atomic level of the behaviour of TOCNF hydrogels in the presence of divalent Zn^{2+} ions, at different salt concentrations, was obtained employing state-of-the-art molecular dynamics (MD) simulations based on a reactive force field appropriately parametrized to describe all the system components. A representative nanofibril model in different ionic solutions was designed using the Zn^{2+}/COO^{-} molar ratio at the different salt concentrations to match the experimental conditions (Table S1†). To create a model as realistic as possible, we estimated the amount of carboxyl groups *via* ^{13}C SS NMR (Fig. S8†) as well as the surface charge density of TOCNF suspension by means of conductometric titration (1.2 mmol g_{TOCNF}^{-1}). Representative snapshots of the simulated nanofibrils at different salt concentrations are shown in Fig. 4.

A series of MD simulations were carried out to disclose the nanofibril structure and dynamics, as well as the effects due to the Zn^{2+} ions on the packing/condensation of the chains. A few results are shown in Fig. 5, and the other data are included in the ESI (Fig. S3, S4 and S9†). The simulations analysis is focused on structural changes of the nanofibril, ions adsorption and solvation effects.

In the final structures of the nanofibrils in water (with Na^{+} counter-ions) most of the Na^{+} ions were stably adsorbed on the cellulose surface, and no significant diffusion was observed after extending the simulation time. Only slight readjustments (spatial displacements <0.2 Å) of the positions of the ions took place to maximize both the contacts with the glucosyl units

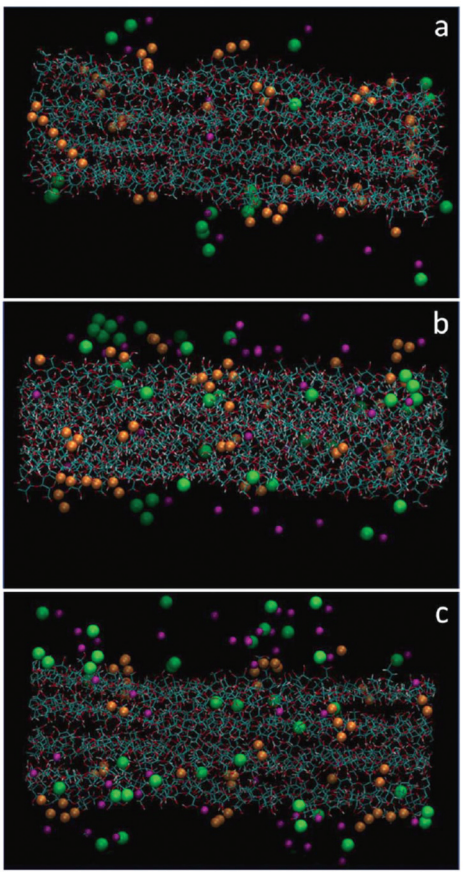

Fig. 4 Representative snapshots of simulated carboxylated cellulose nanofibrils at variable salt concentration: 1 mM (a), 2 mM [C_0] (b) and 3 mM (c). The nanofibrils rendered through dynamic bonds coloured according to the atom type: C = cyan, O = red, H = white, Zn^{2+} = magenta, Na^{+} = orange, and Cl^{-} = green. Water molecules are not displayed for clarity.

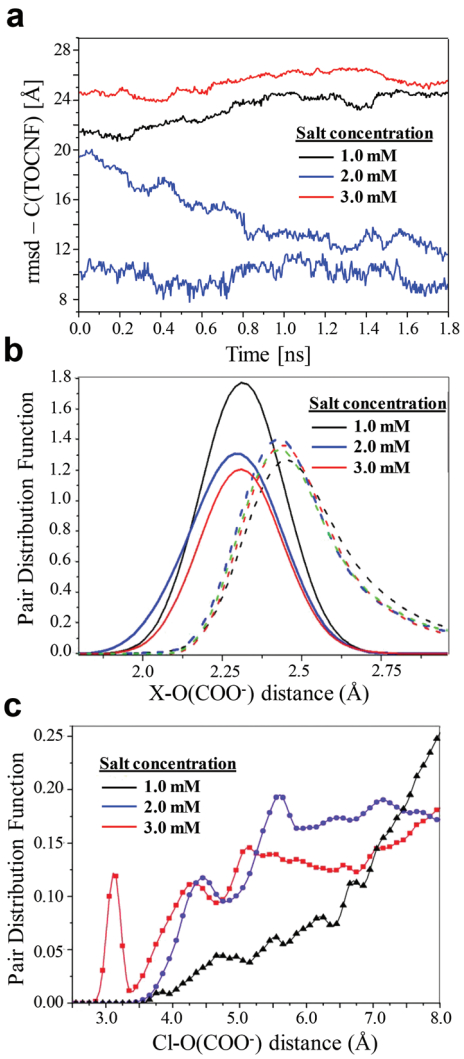

Fig. 5 RMD Simulations of re-entrant transition of TOCNF. (a) Root mean square deviation of the carbon atoms of the TOCNF chains in relation to an average structure obtained from the last 40 ps of the production trajectory of TOCNF in solution with Na^{+} ions only. For 2 mM [C_0] the results obtained from two trajectories are shown. (b) Atom-atom distribution functions between (solid lines) Zn^{2+}-carboxyl oxygens obtained from the last portions of the production trajectories and (dashed lines) Na^{+}-carboxyl oxygens. For comparison, the Na–O(COO) pair distribution function when Zn is not present is represented with dash green lines. (c) Pair distribution functions between the chlorine ions and the oxygen atoms of the carboxyl groups on the nanofibrils.

and self-interactions. This method was used to select all the configurations for the final analysis. The percentage of deprotonated carboxyl groups, Na^+ and Zn^{2+} ions within 3.2 Å of the carboxyl oxygens for all the salt concentrations was evaluated and reported in Table S1† for comparison.

In all the models, the conformation of the nanocellulose chains, which are interconnected through highly dynamic networks of hydrogen bonds involving oxygens and hydroxyl groups, were perturbed by the concerted action of the surrounding water molecules and metal ions that induced a remarkable reorganization of the outer shell of the nanofibrils. The initial tight packing was disrupted and replaced by looser assemblies where water molecules and ions could reach the core of the structure becoming occasional mediators in the hydrogen-bonding networks. It is further important to mention here that we cannot exclude a sort of intrafibrillar CNF rearrangement that could take place because of cationic bridging.[24] However, according to our simulations results, it was found that intrafibrillar changes involved just the outer chains but not the core of the fibril. The effects due to these interactions could be considered minor perturbations compared with the interfibrillar reorganization. Indeed, the ions (in all cases) were found within the chains in contact with the solvent and did not penetrate deep inside the core of the fibril structure.

The more internal chains being less affected by the perturbations of the surrounding solutions, maintained almost elongated geometries. The main effects were found in the edges that twisted and detached from the inner portion of the nanofibril becoming slightly bent. The degree of bending or partial dissociation was mitigated by ion and water penetration. Indeed, it was observed that besides the reduction of the net charge of the nanofibril, the loaded ions weakened the electrostatic repulsion and induced effective attractive interactions. These were responsible for the moderate conformational re-arrangements of the various segments, which determined morphological changes in the nanofibril that stabilized the structures. In agreement with the literature,[49] it was found that local variations of the environment, determined by the presence of different amounts of Zn^{2+} ions in close contact with the cellulose matrix, could markedly affect its conformation and change the whole charge equilibrium of the system. At 1 and 2 mM, the ionization degree of the nanofibril decreased towards less negative values in relation to the one observed in the presence of the monovalent ions only. However, a further increase in salt concentration (3 mM) determined the reappearance of the negative character found when $ZnCl_2$ is not present, (0 mM), which is consistent with the observations of the electrophoretic mobility (Fig. 2c). Inspection of the evolution of the root mean square deviation (rmsd) of the positions of the carbon atoms in the different models relative to the reference structure (in a time interval of about two nanoseconds before stabilization) (Fig. 5a) revealed considerable swelling of the nanofibril at 1 and 3 mM, but the opposite effect, *i.e.* deswelling, at 2 mM, in line with the experimental results.

Based on the classical theories, proposed modifications therein and our simulation results, we propose a plausible mechanism to understand the re-entrant behaviour in TOCNF hydrogels. The initial dispersed state of TOCNF at low salt concentrations goes in good agreement with the Donnan effect, where the increase in the concentration of counter-ions inside the hydrogels gives rise to osmotic pressure imbalance, inducing swelling of the cellulosic hydrogel.[18] This is also supported by the observed pair distribution functions (Fig. 5b) of the Zn^{2+} ions, where increased coordination of Zn^{2+} ions to the carboxyl group is apparent at 1 mM salt concentration.

The collapse of the gel caused by the increase in salt concentration ($C < C_0$) is also expected from the Donnan effect because of the decreasing osmotic pressure difference obtained upon the addition of salt to the reservoir, which may result in the collapse of the hydrogel. Moreover, the weakening of the electrostatic repulsion produced by the reduction of the net charge of the nanofibrils loaded with ions is also an expected and probably dominating cause of the observed collapse of the gel. Indeed, the condensed counter-ions favour attraction between the cellulose chains, as observed in the simulations.

Such collapse continues until the salt concentration of the system attains the critical value [C_0]. Increasing further the concentration of the salt, beyond C_0, did not improve the packing of the gel, which is far from the predictions of the classical Donnan effect and/or other colloidal theories like DH or DLVO theory.[18] It should also be mentioned that this specific behaviour of the system is not contemplated for colloidal systems. Indeed, according to the DH theory, increasing the salt concentration can only result in a systematic collapsing system, due to the monotonic suppression of the Coulomb repulsive barrier.

On the contrary, the inclusion of the inter ion-correlation in the classical assumptions of the Donnan effect can result in the re-entrant of the initial liquid-like state.[18,23] It has been shown theoretically that a gel's over-packing (above the optimal value) is energetically unfavourable due to either electrostatic or hindering effects, if the ion-ion correlations (which are stronger in the case of multivalent ions) are taken into account. Furthermore, the multivalent ions induced re-entrant condensations are also reported for proteins, DNA, nanoparticles and ionic microgels,[17,19,37,38,41] where the presence of multivalent counter-ions re-stabilizes the original structures at higher salt concentrations. In these papers, it was demonstrated that the re-entrance of the initial stable phase happened due to overcharging of the colloids, resulting from excessive condensation of the counter-ions.[19,22,41,50] The ion-ion and ion-macro ion correlations are considered responsible for excessive condensation and hence overcharging.[22] However, in the case of cellulose nanofibrils studied in the present work, no such overcharging is observed. The simulation results at high salt concentrations showed that there was a reduction of the percentage of Zn^{+2} ions, adsorbed on the nanocellulose surface [Table S1† and the electrophoretic mobility also shows slightly more negative values, on further

increase in the salt concentration beyond C_0 (Fig. 2b)]. Analysing the behaviour of the Cl^- ions in the simulations, an enhancement in their coordination to the carboxyl oxygens (at 3 Å distance) is observed, indicating an increased in-flow of the Cl^- ions in the hydrogel probably due to a concentration gradient (Fig. 5c). This enhancement in the in-flow of the Cl^- ions could create an osmotic pressure leading to the re-swelling of the individual fibres, thus leading to the liquid-like (less collapsed) state of the gels. In sum, the re-entrant transition could be partially understood considering modified classical theories (when inter-ion correlations are included) and the observations of our simulation results. However, more rigorous and detailed phenomenological studies considering several other factors such as interfacial ion distribution, specific ion effects, charge distribution on TOCNF, dispersion forces and thermodynamic contributions are required to be carried out to understand the complete phenomenon.[51–53]

The impact of the re-entrant behaviour on the properties of 2D-films (prepared by evaporating the water from the hydrogels with different salt concentrations) was also explored. The emergence of the extraordinary physical properties in CNF films in the presence of multivalent counter-ions has already been reported.[54,55] However, we show here that the observed re-entrant transition can also be translated into the physical properties, proving that this phenomenon could be exploited to design materials with tuneable properties both in the gel and dry state. The variation in the surface topography of the films with different salt concentration was studied by AFM (Fig. S10†), displaying a clear variation in the packing of the nanofibrils upon solvent evaporation at the different aggregated states, which leads to the significant differences in thermal and nano-mechanical stiffness, as well as in wettability, as shown in Fig. 6.

The thermal response of the dried-films was investigated by TGA, and the results are shown in Fig. 6a and b. Interestingly, the degradation profile of the films is significantly influenced by the changes in salt concentration following a trend similar to one of the gelled states. The degradation onset [T_{onset}] shifts towards higher temperatures upon an increment of zinc salt concentration, reaching a maximum at the critical salt concentration [2 mM]. Then, the degradation onset shifts back to lower temperatures upon further addition of metal salt. Surprisingly, the variation in the degradation temperature is of up to 40 °C, as the T_{onset} of the pristine TOCNF film (reference sample, 0 mM $ZnCl_2$), determined by the derivative weight loss (Fig. 6b), is 236.8 °C, which increases to 275.5 °C at 2 mM, to then decrease back to 245.8 °C at 5 mM. This shift is related to a regulation of the nanofibrils assembly and to the morphology of the gel-network, which directly influences the packing and thus, the properties of materials in the dried state. For a better understanding of the morphology evolution during drying, we imaged the hydrogels with varying salt concentration *via* confocal microscopy using Direct Yellow as a stain to visualize the CNF (Fig. S11†). By increasing the concentration, the formation of clusters is observed. Upon drying the clusters tend to adopt more compact structures and eventually aggregate to maximize their interactions and settle in more favourable arrangements (lower energy structures).

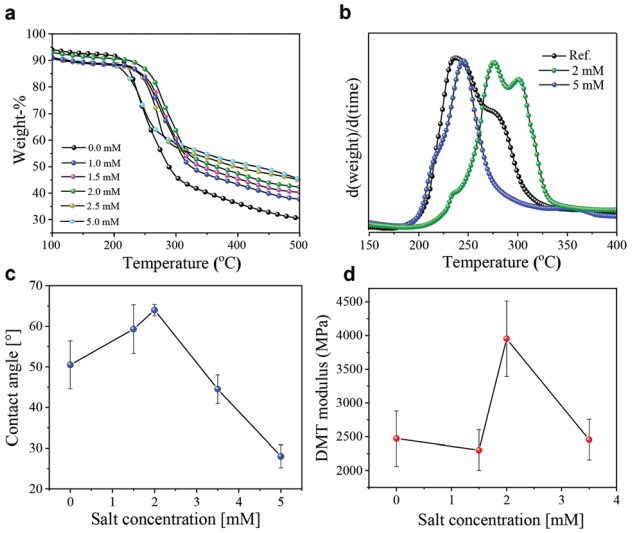

Fig. 6 Influence of the re-entrant transition over the properties of TOCNF dried films. TGA thermogram (a), derivative weight loss (b), contact angle values (measured after 2 seconds of droplet deposition) (c) and DMT modulus (d) of TOCNF with varying salt concentrations. Error bars represent the standard deviation.

The wettability of the TOCNF films was also assessed, and the contact angle values are reported in Fig. 6c. The surface hydrophobicity also follows the trend of the re-entrant behaviour upon varying the salt concentration. The contact angle (after 2 s of droplet deposition) of the TOCNF films increase from 50° (0 mM) to 64° (2 mM [C_0]), to then decrease up to 28° (5 mM) upon further increasing the salt concentration. The hydrophobicity is significantly higher at the critical concentration conditions presumably due to the bigger aggregates that influence the surface roughness of the films, as shown in Fig. S12.† The nano-mechanical stiffness of the films was studied by AFM, and the Derjaguin–Miller–Toporov (DMT) modulus values are shown in Fig. 6d. The DMT modulus enables the determination of surface stiffness with nanoscale resolution in a precise and quantitative manner. The variation in DMT modulus of the films also followed the re-entrant behaviour observed in the gel-state. The pristine TOCNF film exhibit a DMT modulus of ≈2470 MPa which increases as a function of salt concentration reaching a critical value of ≈3950 MPa, at 2.0 mM. Upon further addition of zinc salt, the stiffness decreases back to a modulus of about 2450 MPa at 3.5 mM.

Conclusions

In conclusion, we have identified a multivalent ion-induced re-entrant transition of carboxylated cellulose nanofibrils, observed as an abrupt increase in the gel strength, at a critical salt concentration, which then decreases back upon further

addition of metal ions. We studied this phenomenon by a combination of experimental techniques as well as molecular dynamics simulations. The phenomenon is believed to be emerging due to ion-ion correlations affecting the microstructure and conformation of the nanofibrils, leading to different packing arrangements. These transitions also translated into the properties of 2D-films (upon water evaporation of the hydrogels) which exhibit re-entrant thermal properties, wettability, roughness, and nano-mechanical stiffness. Our findings suggest a prominent application in the design of cellulosic materials with tuneable properties by carefully varying the concentration of multivalent counter-ions, across a small window.

Conflicts of interest

There are no conflicts to declare.

Acknowledgements

The authors thank Hua Guo and Mattias Eden from Stockholm University for their kind support in measuring the ^{13}C SS NMR of TOCNF. S. M. is grateful to the CINECA supercomputing centre for the High-Performance Computing resources provided through the ISCRA initiative. This project has received funding from the European's Union Horizon 2020 research under grant agreement no. 674979-NANOTRANS and 676045-MULTIMAT.

References

1 B. Thomas, M. C. Raj, K. B. Athira, M. H. Rubiyah, J. Joy, A. Moores, G. L. Drisko and C. Sanchez, *Chem. Rev.*, 2018, **118**, 11575–11625.
2 Y. Habibi, L. A. Lucia and O. J. Rojas, *Chem. Rev.*, 2009, **50**, 5438–5466.
3 Y. Xue, Z. Mou and H. Xiao, *Nanoscale*, 2017, **9**, 14758–14781.
4 A. Alanis, J. H. Valdés, N.-V. María Guadalupe, R. Lopez, R. Mendoza, A. P. Mathew, R. de León and L. Valencia, *RSC Adv.*, 2019, **9**, 17417–17424.
5 L. Valencia, V. Arumughan, B. Jalvo, H. J. Maria, S. Thomas and A. P. Mathew, *ACS Omega*, 2019, **4**, 4330–4338.
6 L. Valencia, E. M. Nomena, A. P. Mathew and K. P. Velikov, *ACS Appl. Mater. Interfaces*, 2019, **11**, 16040–16047.
7 L. Valencia, S. Monti, S. Kumar, P. Liu, C. Zhu, S. Yu and A. Mathew, *Nanoscale*, 2019, **11**, 22413–22422.
8 L. Valencia, S. Kumar, B. Jalvo, A. Mautner, G. Salazar-Alvarez and A. P. Mathew, *J. Mater. Chem. A*, 2018, **6**, 16361–16370.
9 H. Fukuzumi, T. Saito, T. Iwata, Y. Kumamoto and A. Isogai, *Biomacromolecules*, 2009, **10**, 162–165.
10 T. H. M. Nguyen, C. Abueva, H. Van Ho, S. Y. Lee and B. T. Lee, *Carbohydr. Polym.*, 2018, **180**, 246–255.
11 H. Lu, M. Behm, S. Leijonmarck, G. Lindbergh and A. Cornell, *ACS Appl. Mater. Interfaces*, 2016, **8**, 18097–18106.
12 P. Liu, K. Oksman and A. P. Mathew, *J. Colloid Interface Sci.*, 2016, **464**, 175–182.
13 L. Valencia and H. N. Abdelhamid, *Carbohydr. Polym.*, 2019, **213**, 338–345.
14 L. Valencia, W. Rosas-Arbelaez, A. Aguilar-Sánchez, A. P. Mathew and A. E. C. Palmqvist, *ACS Appl. Mater. Interfaces*, 2019, **11**, 40424–40431.
15 R. López-Esparza, M. A. Balderas Altamirano, E. Pérez and A. Gama Goicochea, *Adv. Condens. Matter Phys.*, 2015, 683716, DOI: 10.1155/2015/683716.
16 P. Khanjani, H. Kosonen, M. Ristolainen, P. Virtanen and T. Vuorinen, *Cellulose*, 2019, **26**, 4841–4851.
17 F. Bomboi, F. Romano, M. Leo, J. Fernandez-Castanon, R. Cerbino, T. Bellini, F. Bordi, P. Filetici and F. Sciortino, *Nat. Commun.*, 2016, **7**, 1–6.
18 P. K. Jha, W. Zwanikken, M. Olvera and D. Cruz, *Soft Matter*, 2012, **8**, 9519–9522.
19 S. Kumar, I. Yadav, S. Abbas, V. K. Aswal and J. Kohlbrecher, *Phys. Rev. E*, 2017, **96**, 2–6.
20 A. Kubíčková, T. Křížek, P. Coufal, M. Vazdar, E. Wernersson, J. Heyda and P. Jungwirth, *Phys. Rev. Lett.*, 2012, **108**, 186101.
21 J. C. Butler, T. Angelini, J. X. Tang and G. C. L. Wong, *Phys. Rev. Lett.*, 2003, **91**, 28301.
22 A. Y. Grosberg, T. T. Nguyen and B. I. Shklovskii, *Rev. Mod. Phys.*, 2002, **74**, 329–345.
23 C. E. Sing, J. W. Zwanikken and M. Olvera de la Cruz, *Macromolecules*, 2013, **46**, 5053–5065.
24 H. Dong, J. F. Snyder, K. S. Williams and J. W. Andzelm, *Biomacromolecules*, 2013, **14**, 3338–3345.
25 M. Chau, S. E. Sriskandha, D. Pichugin, H. Thérien-Aubin, D. Nykypanchuk, G. Chauve, M. Méthot, J. Bouchard, O. Gang and E. Kumacheva, *Biomacromolecules*, 2015, **16**, 2455–2462.
26 H. Fukuzumi, R. Tanaka, T. Saito and A. Isogai, *Cellulose*, 2014, **21**, 1553–1559.
27 N. Masruchin, B. D. Park, V. Causin and I. C. Um, *Cellulose*, 2015, **22**, 1993–2010.
28 T. Saito and A. Isogai, *Biomacromolecules*, 2004, **5**, 1983–1989.
29 A. Isogai, T. Saito and H. Fukuzumi, *Nanoscale*, 2011, **3**, 71–85.
30 P. A. Hassan, S. Rana and G. Verma, *Langmuir*, 2015, **31**, 3–12.
31 Y. Okita, T. Saito and A. Isogai, *Biomacromolecules*, 2010, **11**, 1696–1700.
32 C. Zhu, S. Monti and A. P. Mathew, *ACS Nano*, 2018, **12**, 7028–7038.
33 H. J. C. Berendsen, J. P. M. Postma, W. F. Van Gunsteren, A. Dinola and J. R. Haak, *J. Chem. Phys.*, 1984, **81**, 3684–3690.
34 N. Mittal, T. Benselfelt, F. Ansari, K. Gordeyeva, S. V. Roth, L. Wågberg and L. D. Söderberg, *Angew. Chem., Int. Ed.*, 2019, **58**, 2–10.

35 P. Bertsch, S. Isabettini and P. Fischer, *Biomacromolecules*, 2017, **18**, 4060–4066.
36 V. L. D. Costa, A. P. Costa and R. M. S. Simões, *BioResources*, 2019, **14**, 7636–7654.
37 S. Kumar, I. Yadav, D. Ray, S. Abbas, D. Saha, V. K. Aswal and J. Kohlbrecher, *Biomacromolecules*, 2019, **20**, 2123–2134.
38 S. Kumar, D. Ray, S. Abbas, D. Saha, V. K. Aswal and J. Kohlbrecher, *Curr. Opin. Colloid Interface Sci.*, 2019, **42**, 17–32.
39 T. T. Nguyen, I. Rouzina and B. I. Shklovskii, *J. Chem. Phys.*, 2000, **112**, 2562–2568.
40 K. Besteman, K. Van Eijk and S. G. Lemay, *Nat. Phys.*, 2007, **3**, 641–644.
41 F. Zhang, M. W. A. Skoda, R. M. J. Jacobs, S. Zorn, R. A. Martin, C. M. Martin, G. F. Clark, S. Weggler, A. Hildebrandt, O. Kohlbacher and F. Schreiber, *Phys. Rev. Lett.*, 2008, **101**, 148101.
42 R. Asor, O. Ben-nun-Shaul, A. Oppenheim and U. Raviv, *ACS Nano*, 2017, **11**, 9814–9824.
43 T. T. Nguyen, A. Y. Grosberg and B. I. Shklovskii, *Phys. Rev. Lett.*, 2000, **85**, 1568–1571.
44 M. Kanduč, M. Moazzami-Gudarzi, V. Valmacco, R. Podgornik and G. Trefalt, *Phys. Chem. Chem. Phys.*, 2017, **19**, 10069–10080.
45 T. Li, A. J. Senesi and B. Lee, *Chem. Rev.*, 2016, **116**, 11128–11180.
46 M. Shibayama, *Soft Matter*, 2012, **8**, 8030–8038.
47 M. Shibayama, *Polym. J.*, 2011, **43**, 18–34.
48 Y. Zhou, S. Fujisawa, T. Saito and A. Isogai, *Biomacromolecules*, 2019, **20**, 750–757.
49 V. S. Rathee, H. Sidky, B. J. Sikora and J. K. Whitmer, *J. Am. Chem. Soc.*, 2018, **140**, 15319–15328.
50 D. Truzzolillo, S. Sennato, S. Sarti, S. Casciardi, C. Bazzoni and F. Bordi, *Soft Matter*, 2018, **14**, 4110–4125.
51 T. Benselfelt, M. Nordenström, M. M. Hamedi and L. Wågberg, *Nanoscale*, 2019, **11**, 3514–3520.
52 G. Trefalt, T. Palberg and M. Borkovec, *Curr. Opin. Colloid Interface Sci.*, 2017, **27**, 9–17.
53 M. Kanduč, M. Moazzami-Gudarzi, V. Valmacco, R. Podgornik and G. Trefalt, *Phys. Chem. Chem. Phys.*, 2017, **19**, 10069–10080.
54 T. Benselfelt, M. Nordenström, S. B. Lindström and L. Wågberg, *Adv. Mater. Interfaces*, 2019, **6**, 1900333.
55 M. Shimizu, T. Saito and A. Isogai, *J. Membr. Sci.*, 2016, **500**, 1–7.
56 E. J. Baerends, *et al.*, *ADF, adf2014.05 SCM, Theoretical Chemistry*, Vrije Universiteit, Amsterdam, The Netherlands, http://www.scm.com.